Unstable Transition of the Tropical Climate to an Equatorially Asymmetric State in a Coupled Ocean–Atmosphere Model

SHANG-PING XIE

Graduate School of Environmental Earth Science, Hokkaido University, Sapporo, Japan

(Manuscript received 30 March 1995, in final form 7 November 1995)

ABSTRACT

Over a large zonal extent of the central and eastern Pacific, the intertropical convergence zone (ITCZ) is located to the north of the equator. Collocated with this ITCZ is a zonal band of warm sea surface, where the highest sea surface temperatures (SST) along a meridian are found. A one-dimensional coupled ocean–atmosphere model that neglects zonal variations is used to investigate this problem of latitudinal asymmetry in the tropical climate. The equatorially symmetric model solution is found to be unstable to infinitesimal disturbances and equatorial asymmetries develop spontaneously. A linear instability that is stationary in space and antisymmetric about the equator is responsible for the unstable transition of the model from the symmetric state. The destabilizing mechanism involves a positive feedback between the scalar wind speed and SST through surface evaporation, which is illustrated with a simple low-order model that contains only two SST grid points, one in each hemisphere.

The existence of the equatorially antisymmetric instability indicates that in a zonally uniform setting, a latitudinally asymmetric climate with a single ITCZ off the equator could emerge on a symmetric planet.

1. Introduction

In the Tropics, deep convection is organized in space and appears on time-average maps as zonal bands with narrow meridional extents. The heat associated with the solar radiation is the ultimate energy source for the tropical deep convection. This forcing and response relation suggests that the distribution of tropical convective activity should be determined by that of the solar radiation and be symmetric about the equator, as indeed observed over land, as well as the Indian and western Pacific Oceans. Exceptions occur in the eastern Pacific and Atlantic, where convection is active in the Northern but suppressed in the Southern Hemisphere. The correlation between the convective activity and the solar radiation breaks, because most of the solar energy is absorbed at the earth's surface, and over the ocean the sea surface temperature (SST) modifies the heat flux into the atmosphere and determines the static stability of the atmosphere. Consistent with this reasoning, the intertropical convergence zone (ITCZ) and a zonal band of high SST are found to be collocated with each other in the Atlantic and eastern Pacific, indicating that the ocean–atmosphere interaction is essential for maintaining an equatorially asymmetric ITCZ. This argument is further reinforced by ocean and atmosphere general circulation model (GCM) experiments; the formation of a northerly ITCZ requires the high SST to appear in the Northern Hemisphere (Manabe et al. 1974), while the wind field associated with a northerly ITCZ leads to a collocated, northerly SST maximum (Xie 1994a).

Recently, Xie and Philander (1994; XP hereafter) proposed an SST–wind feedback mechanism for the maintenance of an equatorially asymmetric ITCZ. If an ITCZ forms in the Northern Hemisphere, the veering of the convergent winds by the Coriolis force weakens the prevailing easterly trades between the equator and the ITCZ but enhances the easterlies to the south of the equator. This latitudinally asymmetric distribution of the wind speed leads to an SST distribution that is asymmetric about the equator since the latent heat flux from the ocean, a function of both SST and wind speed, has to balance the symmetric solar radiation absorbed at the ocean surface. This equatorially asymmetric SST distribution, with high SST in the Northern but low SST in the Southern Hemisphere, decides that the ITCZ should continue to stay in the Northern Hemisphere. By this mechanism, a pair of solutions, which are asymmetric about the equator with the ITCZ and the high SST band appearing only in one hemisphere, are found in simple (XP) and hybrid (Xie 1994b) coupled ocean–atmosphere models under latitudinally symmetric conditions. Xie and Philander (1994) speculate that the geographic asymmetries between the hemispheres, such as those in the land mass distribution and the orientation of coastal lines, be responsible for selecting the Northern Hemisphere mode of the ITCZ in the current earth cli-

Corresponding author address: Dr. Shang-Ping Xie, Graduate School of Environmental Earth Science, Hokkaido University, Sapporo 060, Japan.
E-mail: xie@eoas.hokudai.ac.jp

mate. They further show that the existence of the asymmetric solutions requires cooling at the equator by oceanic upwelling. Only when the cooling by the upwelling is strong enough to prevent the ITCZ from forming on the equator the wind–SST feedback mechanism through evaporation leads to asymmetric steady states. This necessary condition for the equatorially asymmetric solutions is consistent with observed zonal variation in the meridional distribution of the ITCZ. The persistent northerly ITCZ is seen only in the Atlantic and eastern Pacific where the equatorial upwelling cools the equator, whereas nearly symmetric ITCZ is observed in the Indian and western Pacific where the effects of upwelling/downwelling are weak on SST.

Besides the asymmetric solutions, an equatorially symmetric solution with a meridional distribution of SST similar to that of the solar radiation is also possible. When the upwelling cooling near the equator is weak, XP show that the symmetric solution is the only solution to the model. It will be shown in the next section that in the regime where the asymmetric solutions are possible, the symmetric solution is unstable. An equatorially antisymmetric linear instability, due to a wind–evaporation–SST feedback similar to that operating in the steady-state solution, dominates the process of transition from the symmetric to the asymmetric solution. The unstable nature of the equatorially symmetric state, which has been previously reported in a three-dimensional hybrid coupled ocean GCM (Xie 1994b), can be understood in a very simple context of a one-dimensional model. It is the purpose of this study to describe this instability and to investigate its unstable mechanism. The fact that this instability occurs in two models with different configurations (one- vs three-dimensional) and different physics (a slab ocean with no active dynamics versus a full GCM) suggests that this instability may also occur in other models. The approach of this study can be used to test the existence of this asymmetrizing instability in other models including coupled GCMs. Such a test could answer the basic question of whether the coupled ocean–atmosphere system allows a latitudinally asymmetric state under symmetric conditions.

Equatorial upwelling and downwelling play important roles in maintaining the cold tongue and in generating the El Niño–Southern Oscillation (ENSO). Because of prevailing geostrophy, oceanic vertical motion is suppressed at the latitude of the ITCZ, which is a few oceanic radii of deformation away from the equator. There is observational evidence suggesting that upwelling/downwelling acts to reverse the observed latitudinal asymmetry of SST associated with the ITCZ. As XP point out, there is a weak upwelling at the location of the ITCZ that tends to cool the upper ocean, whereas there is a downwelling at 10°S on the other side of the equator (see their Fig. 1). The former is caused by the positive curl of the converging winds, whereas the latter is caused by the equatorial upwelling.

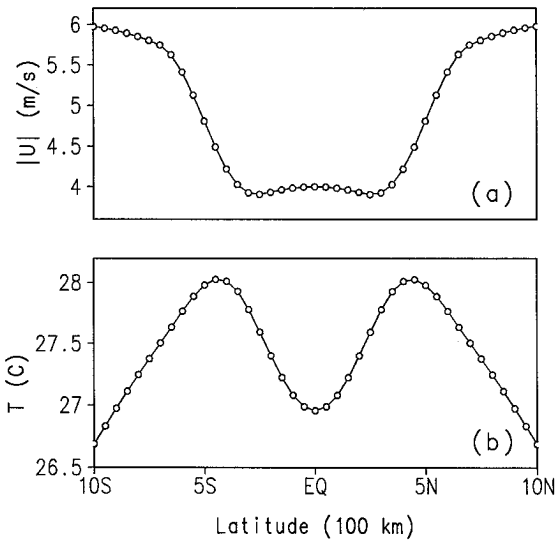

FIG. 1. (a) Scalar wind speed and (b) sea surface temperature in the equatorially symmetric steady-state solution as functions of latitude.

Within the equatorial radius of deformation (≈300 km), upwelling/downwelling does play a role in establishing another latitudinal asymmetry—the equatorial upwelling is not centered on the equator but 1° or 2° to the south. Indeed, Chang and Philander (1994) show that a coupled instability involving upwelling/downwelling can cause the center of the cold tongue to shift away from the equator. As seen in the above, upwelling/downwelling could have very different effects on the latitudinal asymmetry at different meridional scales. This paper concerns the larger-scale latitudinal asymmetry, that is, that of the ITCZ between 10°S and 10°N. For this purpose, the small departure of the center of equatorial upwelling from the equator may be neglected. Following XP, we will parameterize the upwelling cooling with a symmetric function of latitude. This upwelling parameterization is supported by ocean GCM experiments in which large latitudinal asymmetry persists under symmetric ocean upwelling (Xie 1994a,b). This simplification enables us to focus on the symmetry-breaking effect of the wind–evaporation–SST feedback.

The rest of the paper is organized as follows. Section 2 describes the unstable transition to the asymmetric solution. Section 3 examines the linear instability with the help of a simple low-order model. Section 4 extends the analysis to a case with a different coupling procedure. Section 5 summarizes the study.

2. Unstable transition from the symmetric solution

Xie and Philander's (1994) coupled model is one-dimensional, neglecting the change in the zonal direction. Its atmospheric component is a Matsuno–Gill-type model:

$$\epsilon u - YV = 0, \tag{2.1}$$

$$\epsilon V + Yu = -\Phi_Y, \tag{2.2}$$

$$\epsilon\Phi + V_Y = -Q, \tag{2.3}$$

where u and V are the zonal and meridional low-level wind velocities; Φ is the geopotential; $Y = y(\beta/C)^{1/2}$ is the nondimensional meridional coordinate; $\epsilon = A(\beta C)^{-1/2}$ is the nondimensional damping rate, with A being its dimensional counterpart, C is the atmospheric long gravity wave speed, and β is the latitudinal gradient of the Coriolis parameter. To mimic the easterly winds by the eddy momentum transport and the zonal contrast between the warm pool and the cold tongue, a constant zonal wind, $U_0 = -4$ m s^{-1}, is added to the model output so that the zonal wind used to drive the ocean is

$$U = U_0 + u. \tag{2.4}$$

Latent heating released to the atmosphere by deep convection is parameterized as a function of SST with a threshold, T_c,

$$Q = \frac{K_Q}{(\beta C^3)^{1/2}}(T - T_c)H(T - T_c), \tag{2.5}$$

where $H(x)$ is the Heaviside function and K_Q the thermal coupling coefficient. Such a step function dependence of deep convective activity on SST is observed in the Tropics.

The ocean contains a slab mixed layer whose temperature T is governed by

$$\frac{\partial T}{\partial t} = \frac{Q_0 - Q_w - C_E^*|\mathbf{U}|q(T)}{\rho c_p h} + \kappa\frac{\partial^2 T}{\partial y^2}, \tag{2.6}$$

where h is the mixed-layer depth, ρ and c_p are the water density and specific heat, Q_0 is the radiative flux, C_E^* is the evaporation efficiency coefficient, $q = q_0 \exp[LR^{*-1}(T_0^{-1} - T^{-1})]$ is the saturated specific humidity given by the Clausius–Clapeyron equation, κ is the diffusivity, and y the dimensional coordinate. The cooling by the equatorial upwelling and the poleward advection is parameterized as an equatorially trapped, symmetric function of latitude, $Q_w = Q_w^0 \exp[-0.5(y/300\text{ km})^2]$. As a result, the atmosphere can affect the ocean only through the wind speed dependence of surface evaporation. The ocean extends from 30°S to 30°N and the atmosphere from 45°S to 45°N. Conditions of zero heat flux and vanishing V are applied at the poleward boundaries. For details of the derivation readers are referred to XP. In this study $h = 50$ m is used, a value representative of the tropical eastern Pacific. All other parameters are the same as in XP, including $K_Q = 1.2 \times 10^{-2}$ m^2 s^{-3} K^{-1} and $\kappa = 2 \times 10^3$ m s^{-2}.

The symmetric solution can be obtained by running the model in a hemispheric configuration and imposing equatorially symmetric boundary conditions, $V = 0$ and $\partial T/\partial y = 0$, at the equator. Figure 1 depicts the spatial structures of the symmetric solution. SST has a minimum at the equator due to the imposed upwelling cooling Q_w, with two symmetric maxima off the equator. In response to the double ITCZs, the easterly winds weaken slightly near the equator but then increase poleward. After the steady-state symmetric solution is obtained, the symmetric boundary conditions at the equator are then removed and the model is run in the full domain that covers both hemispheres. Figure 2a shows the time–latitude evolution of this symmetric solution. For the first 10 years, there are no visible changes in the SST structure. The meridional wind speed at the equator, whose logarithm is depicted in Fig. 2b as a function of time, is a more sensitive index of the equatorial asymmetry than the total SST since it vanishes in the symmetric solution. After a period of adjustment shorter than a year, the meridional wind speed at the equator grows exponentially, indicating that latitudinal asymmetries are building up rapidly. The numerical model is perfectly symmetric about the equator and the initial asymmetries arise from machine's round-off errors. The exponential growth of this small asymmetric disturbance indicates that the symmetric solution is unstable. The growth rate of the dominant instability mode is 2.8 yr^{-1}. The initial wind perturbation is so small ($v|_{y=0} \approx e^{-35}$ on a double-precision machine) that its effect is not visible in the plot of the total SST (Fig. 2a). As this instability grows with time into large amplitudes, the asymmetries in the SST eventually become visible around year 10 from the time–latitude section, and the time evolution of $\log|v|$ departs from the straight line of the exponential growth in Fig. 2b. Around year 11, drastic changes occurs in SST; it warms up in the Southern and cools rapidly in the Northern Hemisphere. Correspondingly, the meridional wind anomaly at the

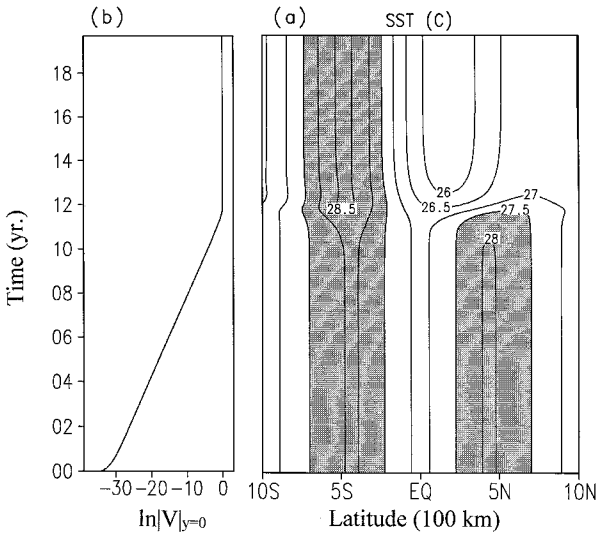

FIG. 2. (a) Time–latitude section of sea surface temperature and (b) logarithm of the meridional wind speed at the equator as a function of time in the nonlinear XP model. The slope of the curve in (b) gives the growth rate.

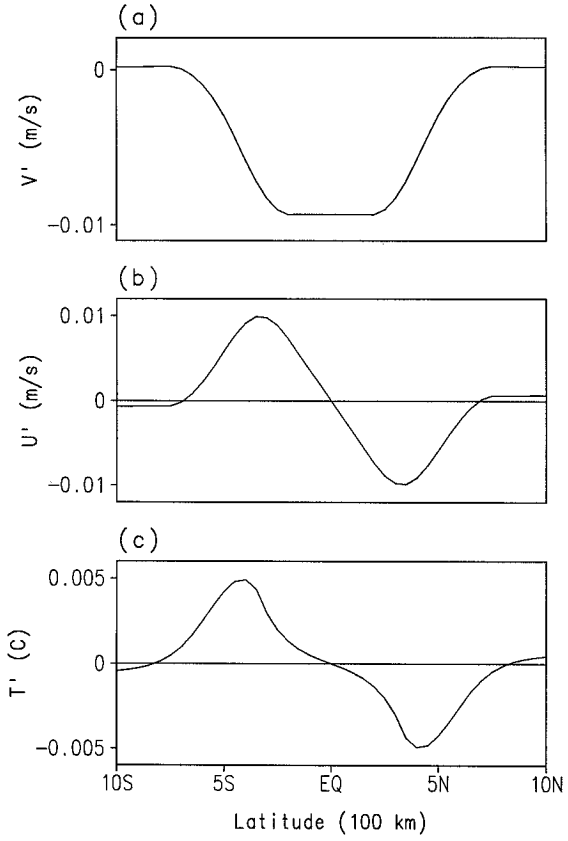

FIG. 3. Deviations from the equatorially symmetric solution of (a) meridional and (b) zonal wind velocities and (c) sea surface temperature on year 10 of Fig. 2 as functions of latitude.

equator is approaching a constant. All these indicate that nonlinearities have phased in to stop the unstable growth. The most important among these nonlinearities is the one associated the SST criterion for deep convection, which limits the area of oceanic feedback to the atmosphere. The convective regions do not change much for the first 11 years, but the continuous decrease in the Northern Hemisphere SST suppresses the ITCZ in the Northern Hemisphere, triggering the final stage of rapid transition to the asymmetric solution. At the end of the model run, an asymmetric solution similar to that described in XP is established.

Figure 3 shows the model deviations from the initial symmetric solution on day 3600, which basically represent the meridional structures of the dominant instability mode. The mode is antisymmetric about the equator with the maximum SST anomalies at 4° latitude. In response to this antisymmetric structure of SST deviation, northerly wind anomalies prevail in the equatorial region, converging onto the positive SST anomaly in the Southern Hemisphere. These northerly winds induce easterlies in the Northern and westerlies in the Southern Hemisphere, with the phase of the zonal wind anomaly nearly coinciding with that of the SST anomaly. Since the easterly winds prevail in the symmetric solution that is the mean state for the instability, the anomalous easterlies enhance surface evaporation and thus cool the ocean mixed layer, intensifying the negative SST anomalies in the Northern Hemisphere. This loop of SST → wind → evaporation → SST forms a positive feedback, which works the same way in the Southern Hemisphere to amplify the disturbance. Hereafter, we will call this feedback wind–evaporation–SST (WES) feedback.

Similar unstable departure from the symmetric solution is observed in the other version of XP's model that includes a reduced-gravity ocean dynamics and an explicit ocean mixed layer dynamics. Both the temporal and spatial structures of the unstable transition are similar to what is described above, except that the wind stirring effect, proportional to the cubic of the wind speed, enhances the positive feedback. All the results in this paper can be extended to this model with more ocean physics. For this particular coding of the model equations, round-off errors generate negative and positive SST anomalies in the Northern and Southern Hemispheres, respectively. When a small positive SST perturbation is put in the Northern Hemisphere, the same unstable transition occurs, with the signs of anomalies in Fig. 3 reversed though.

All results presented in this paper are from calculations using double precision numbers. In XP's original calculations single precision numbers were used and SST (K) was calculated, reducing the significant digits of model SST. The asymmetry in wind speed induced by round-off errors is so small that the SST asymmetry it causes cannot be represented with single precision numbers. The lack of enough significant digits for SST leaves the symmetric solution stable in XP's calculations for certain parameter ranges.

3. Linear stability analysis

The unstable transition described above can be understood by analyzing the stability of the symmetric solution to infinitesimal disturbances. With the overbar and the prime denoting the symmetric solution and the departure from it, respectively, the term $|\mathbf{U}|q(T)$ may be decomposed as

$$|\mathbf{U}|q(T) = -\overline{Uq} - U'\overline{q} + \frac{L}{R^*\overline{T}^2}\overline{Uq}T' + o(T'^2, U'T', V'^2), \tag{3.1}$$

where $|\overline{U} + U'| = -\overline{U} - U'$ for large negative $\overline{U}$ is used. In the equatorially symmetric solution, the meridional wind speed is an order of magnitude smaller than the zonal wind speed and vanishes at the equator and at the centers of the double ITCZ (see XP's Fig. 2a). We could then effectively set $\overline{V} = 0$. As a result, the contribution of the meridional wind perturbation to the total wind speed is a higher-order effect and can be neglected. From (2.6) and (3.1), a linearized equation for perturbation temperature is obtained:

$$\frac{\partial T}{\partial t} = aU' - bT' + \kappa \frac{\partial^2 T'}{\partial y^2}, \tag{3.2}$$

where prime denotes the deviation from the basic state,

$$a = \left(\frac{1}{-\overline{U}}\right)\frac{E}{c_p \rho h}, \tag{3.3a}$$

$$b = \left(\frac{L}{R^* \overline{T}^2}\right)\frac{\overline{E}}{c_p \rho h}, \tag{3.3b}$$

and $\overline{E} = C_E^* |\overline{U}| q(\overline{T})$ is the evaporation rate in the basic state.

Xie and Philander (1994) found that the SST threshold for deep convection (T_c) is crucial for their asymmetric solutions. Anomalous heating to the atmosphere occurs only in convective regions with SST exceeding the threshold

$$Q' = \frac{K_Q}{C(\beta C)^{1/2}} T' H(\overline{T} + T' - T' - T_c). \tag{3.4}$$

With L being the latitudinal extent of heating in the basic state, the anomalous heating due to the temperature change, Q_T, is on the order of $T'L$. Temperature change will cause change in the boundaries of convective region, unless T' vanishes on these boundaries. The change in the extent of heating is $T'L(T_0 - T_c)^{-1}$, with $(T_0 - T_c)L^{-1}$ being the temperature gradient within the convective region and T_0 the maximum temperature. We can then estimate the heating anomaly due to the change in the boundaries of convective region, $Q_L \propto T'^2 L(T_0 - T_c)^{-1}$. As a result, $Q_L/Q_T = T'/(T_0 - T_c) \ll 1$. In other words, the effect of change in the boundaries of the convective region is negligible for infinitesimal disturbances. The Heaviside function in (3.4) may thus be linearized and replaced with a function of latitude:

$$F(Y) = \begin{cases} 1, & Y_E \le |Y| < Y_P, \\ 0, & \text{otherwise}, \end{cases} \tag{3.5}$$

where Y_E and Y_P are the equatorward and poleward boundaries of the convective region in the Northern Hemisphere. Consequently, the expression for anomalous heating rate (3.4) becomes

$$Q' = \frac{K_Q}{C(\beta C)^{1/2}} T' F(Y). \tag{3.6}$$

Thus active ocean–atmospheric coupling is confined to two latitudinal bands astride the equator.

Simple manipulation of the Matsuno–Gill model equations yields

$$\frac{\partial^2 V}{\partial Y^2} - (Y^2 + \epsilon^2)V = -\frac{\partial}{\partial Y}(F\Theta) \tag{3.7a}$$

or its simpler form under the ''long wave'' approximation for $\epsilon^2 \ll 1$,

$$\frac{\partial^2 V}{\partial Y^2} - Y^2 V = -\frac{\partial}{\partial Y}(F\Theta). \tag{3.7b}$$

With the help of (2.1), (3.2) becomes

$$\frac{\partial \Theta}{\partial t} = \lambda Y V + \kappa^* \frac{\partial^2 \Theta}{\partial Y^2}, \tag{3.8}$$

where

$$\Theta \equiv \frac{K_Q}{C(\beta C)^{1/2}} T', \tag{3.9}$$

$$\lambda = \frac{aK_Q}{AC} = \text{sign}(-\overline{U})\frac{q(\overline{T})}{c_p \rho AC}\frac{C_E^* K_Q}{h}, \tag{3.10}$$

and $\kappa^* = \kappa C/\beta$. Note that the coupling coefficient λ is inversely proportional to the mixed layer depth. In (3.8), the Newtonian cooling term has been dropped for clarity, which reduces the growth rate by b without affecting the linear solution qualitatively. In fact, it can be formally removed by making variable transformation $\Theta = \Theta^* e^{-bt}$.

Strictly speaking, λ varies with latitude due to the nonlinearity of the Clausius–Clapeyron equation. The variation in λ is small, however, since the basic SST changes only about 1°C in Fig. 1. A spatially constant value of λ is thus used, estimated using a constant SST of 30°C. The most important effect of the spatial variations in the basic-state SST is represented by $F(Y)$, which limits cumulus heating to windows $Y_E < |Y| < Y_P$ where $\overline{T} > T_c$. If not stated otherwise, the boundaries of the coupling window are chosen to be $Y_P = 800$ km and $Y_E = 0$ in this section. The position of the equatorial boundaries of the coupling windows affect only the growth rate qualitatively as will be discussed briefly in the next subsection. Replacing the steep step function (3.5) with a smooth hyperbolic tangent function yields qualitatively the same results.

The linear model equations, (3.7) and (3.8), which contain a spatially varying coefficient $F(Y)$, are solved numerically with the same finite difference schemes as in XP. In this paper, numerical solutions to the linear system (3.7a) and (3.8) are shown. With finite diffusivity, numerical solutions show little change when the long-wave approximation form (3.7b) is used instead.

a. Antisymmetric instability

An instability that is spatially stationary and antisymmetric about the equator is found in this linear system with a finite coupling window $|Y| < Y_P = 800$ km. Its growth rate is estimated to be 4.5 yr^{-1}. The spatial structures of this linear instability, shown in Fig. 4, resemble those of anomalies in the nonlinear full model in Fig. 2. The WES feedback described in section 2 is responsible for the unstable growth. The zonal wind induced by the cross-equatorial meridional wind changes direction across the equator, amplifying the equatorially antisymmetric SST disturbances that produce the merid-

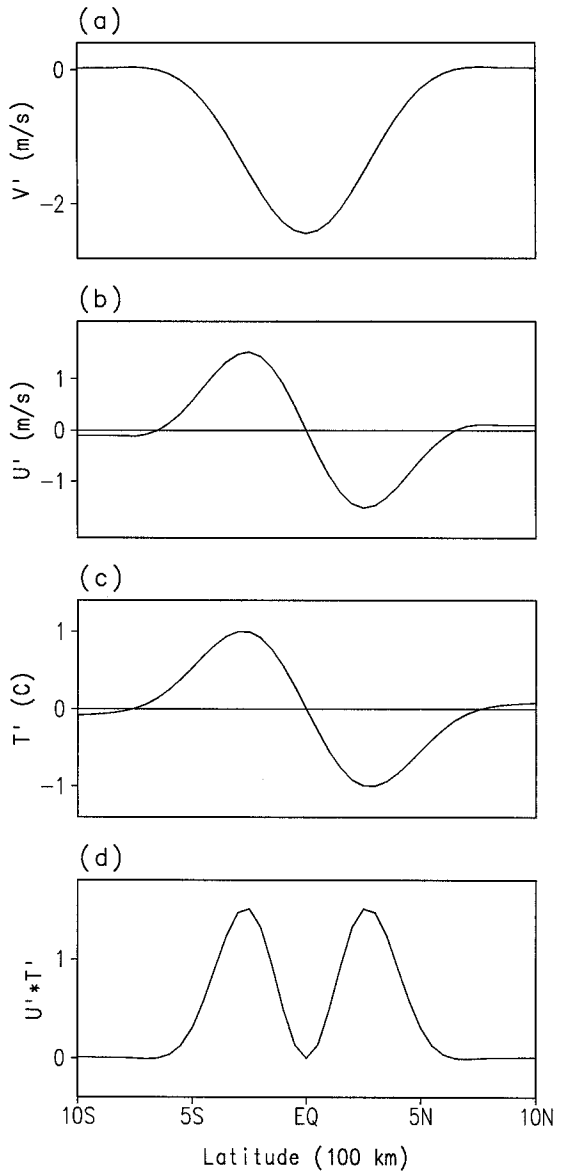

FIG. 4. (a) Meridional and (b) zonal wind velocities, (c) sea surface temperature, and (d) destabilizing term $U'T'$ as functions of latitude.

ional wind. A variance equation for SST can be easily derived, which is helpful for understanding the destabilizing process. Multiplying (3.1) with T' and integrating it over the oceanic domain lead to

$$\frac{1}{2}\frac{\partial}{\partial t}\overline{T^2} = a\overline{U'T'} - b\overline{T'^2} - \kappa\overline{\left(\frac{\partial T'}{\partial y}\right)^2}, \qquad (3.11)$$

where the overbar denotes the area integral. It follows that for a temperature disturbance to grow with time, the term $U'T'$ integrated over the whole domain must be positive. Figure 4d depicts the spatial distribution of this destabilizing term, which is positive in most part of the domain since U' and T' are in phase nearly everywhere. The double bell shape is typical of the distribution of the product of two antisymmetric variables with the same phase.

In the nonlinear full model, a minimum wind requirement is imposed in calculating evaporation to mimic the effects of high-frequency atmospheric disturbances; the wind speed is set to be this minimum value (4 m s^{-1}) whenever the former is smaller than the latter. This is a nonlinearity that is not considered in the above analysis, but it can be linearized for the same reason that leads to the linearized expression (3.5). As a result, not only the area of oceanic feedback to the atmosphere is limited by (3.5), the feedback from the atmosphere is also confined to a window determined by the minimum wind requirement. More specifically, the wind speed anomalies near the equator do not affect surface evaporation since the winds are weaker than the minimum wind in the symmetric solution (Fig. 1a). In other words, another coupling window F_W needs to be introduced so that

$$\frac{\partial \Theta}{\partial t} = \lambda F_W Y V + \kappa^* \frac{\partial^2 \Theta}{\partial Y^2},$$

where

$$F_W(Y) = \begin{cases} 1, & |Y| < Y_W, \\ 0, & \text{otherwise.} \end{cases}$$

The case presented so far corresponds to $Y_W = 0$. To confirm its ability to reproduce the details of the instability seen in the nonlinear model, the linear model is run with all the three window boundaries, Y_E, Y_P, and Y_W, derived from the symmetric solution shown in Fig. 1. The spatial structures of the linear instability mode are indistinguishable from those of the anomalies derived from the nonlinear model (not shown). The growth rate of the linear mode, corrected by the Newtonian cooling, is 2.75 yr^{-1}, in close agreement with the estimation from the nonlinear model.

We now return to the simpler case with $Y_E = 0$ and $Y_W = 0$. Figure 5a shows the growth rate of the WES instability as a function of coupling coefficient K_Q. The dashed line indicates the size of the Newtonian cooling rate, $b = 1$ yr^{-1}. The growth rate increases with the coupling strength. The rate of increase, however, is not a constant, but decreases as K_Q increases. The spatial structures of the instability also change with K_Q. Figure 5b depicts the meridional SST structures of the instability modes for two different K_Q. The instability has a broader meridional scale with a smaller value of K_Q; the maximum temperature moves poleward from 3° latitude to 4° with the smaller K_Q. A broader meridional structure leads to a larger rate of increase with K_Q in the growth rate. If the Newtonian damping is taken into account, the growth rate of the WES mode for small values of K_Q is negative. As a consequence, the symmetric solution is stable and any asymmetric initial conditions are damped back toward the stable symmetric solution

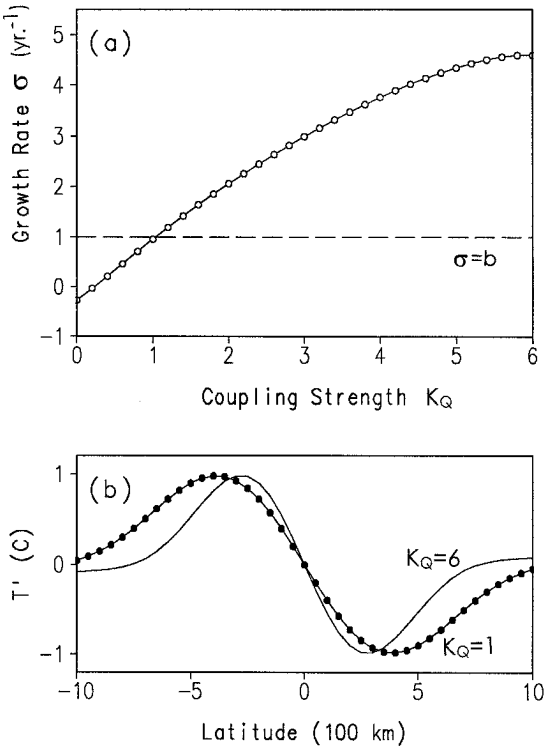

FIG. 5. (a) Growth rate σ of the antisymmetric instability as a function of K_Q (2×10^{-3} m^2 s^{-3} K^{-1}). The dashed line shows $\sigma - b = 0$, the neutral point for the WES mode in the nonlinear full model. (b) Meridional structure of the instability modes with coupling coefficients $K_Q = 2 \times 10^{-3}$ (line with dots) and $K_Q = 1.2 \times 10^{-2}$ m^2 s^{-3} K^{-1}.

in the full nonlinear model. In the limiting decoupling case with $K_Q = 0$, the solution to the nonlinear model is obvious and uniquely determined by the solar radiation and background wind U_0.

The abscissa of Fig. 5a can be interpreted to be the effective coupling coefficient $\lambda \propto K_Q/h$ [see (3.10)]. The growth rate as a function of K_Q and h can be mapped with the information in Fig. 5a. Such a map is shown in Fig. 6 for the growth rate corrected by the Newtonian damping effect, $\sigma' = \sigma(K_Q/h) - b(h)$, where σ is the growth rate for $b = 0$. The corrected growth rate σ' is what one observes in the nonlinear full model. The general increasing trend of the growth rate with coupling strength K_Q remains. Its dependence on the mixed-layer depth, however, exhibits two regimes. For a small coupling coefficient or a very shallow mixed layer, σ' is generally negative and increases with h. The second regime, with σ' positive, is more relevant to the problem of latitudinal asymmetry. Here, as the mixed layer deepens, the effect of the reduction in the effective coupling coefficient λ is dominant and, as a result, the growth rate decreases. In addition to the deep mixed layer, the growth rate is further reduced by the shrink of the coupling window in the western Pacific. The annual mean easterlies are very weak there between 10°N and 10°S,

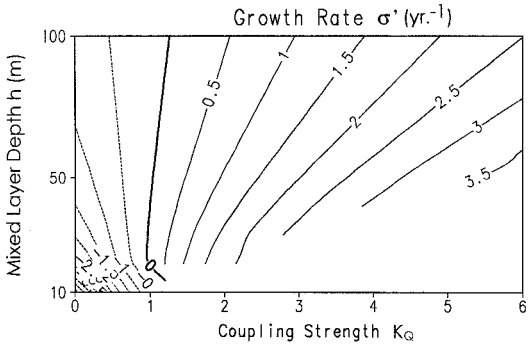

FIG. 6. Growth rate adjusted by the Newtonian cooling effect, $\sigma' = \sigma - b$, as a function of K_Q and h. Negative contours are dashed.

shielding out the atmospheric feedback to the ocean. The combined effects of the deep mixed layer and weak easterlies are likely to stabilize the WES mode and explain the latitudinal symmetry in SST in the western Pacific. Consistent with this argument, the zonal variation in the latitudinal asymmetry is reproduced in a three-dimensional hybrid GCM, which contains the same asymmetry generating mechanism (Xie 1994b).

A finite diffusivity is necessary to obtain the spatially stationary mode. As κ approaches zero, the meridional scale of the mode becomes small, and equatorward propagating modes appear, which will be described in the next section. Figure 7a shows the growth rate of the stationary WES mode as a function of κ. For inter-

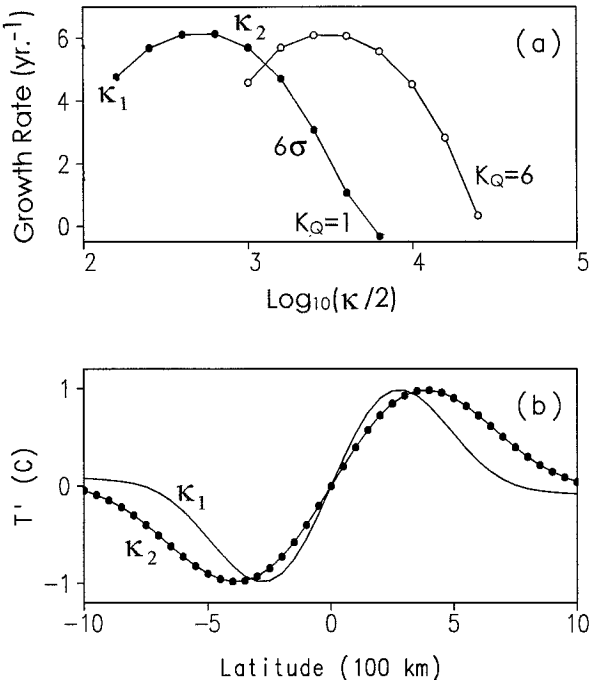

FIG. 7. (a) Growth rate σ as functions of diffusivity κ. A factor of 6 is multiplied to the curve for $K_Q = 1 \times (2 \times 10^{-3})$ to show the similarity of the two curves. (b) Meridional structures of the WES mode for two different values of diffusivity, $\kappa_2 > \kappa_1$.

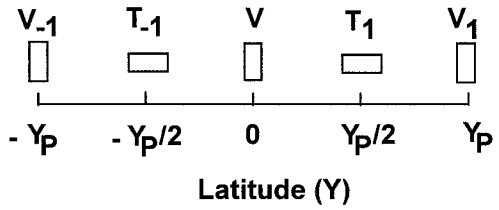

FIG. 8. Grid system for the low-order model.

mediate values of κ, the growth rate increases with κ due to the increase in the meridional scale of the modal structure (Fig. 7b). As κ further increases, its damping effect dominates and the growth rate decreases. It is interesting to note that parameters κ and λ can be combined into a single one. Dividing (3.8) with κ yields

$$\frac{\partial \Theta}{\partial t^*} = \lambda^* Y V + \frac{\partial^2 \Theta}{\partial Y^2}, \tag{3.12}$$

where $t^* = \kappa^* t$, $\lambda^* = \lambda/\kappa^*$. The growth rates obtained from the model calculation for two different values of κ are plotted together in Fig. 7a. The similarity between the two curves is obvious. A commonly used value of $\kappa = 2 \times 10^3\ \mathrm{m^2\ s^{-1}}$ falls in the regime where the growth rate is insensitive to changes in κ.

b. Low-order model

The unstable modes in Figs. 3 and 4 have simple meridional structures. The knowledge of such modal structures can simplify the model greatly, yielding a better understanding of the WES instability. Here, we take an approach of finite differencing the model equations on the staggering grid system that contains the minimum grid points necessary to describe the modal structures (Fig. 8). One grid point for T and U is placed in each hemisphere to capture the off-equatorial extreme. The equatorial grid point is to capture the maximum meridional wind speed of the antisymmetric mode. The off-equatorial V points are chosen to be at $\pm Y_P$, the poleward boundaries of the coupling window. Heating to the atmosphere vanishes and wind perturbations are very small for $|Y| > Y_P$ for the antisymmetric mode, as is clear from Figs. 3 and 4. It follows that approximately

$$V_1 = V_{-1} = 0. \tag{3.13}$$

Applying the center difference to (3.7b) and (3.8) with the help of (3.13) yields

$$V = \frac{Y_P}{2}(\Theta_1 - \Theta_{-1}), \tag{3.14}$$

$$\frac{\partial \Theta_1}{\partial t} = \lambda Y_P \frac{V}{4}, \tag{3.15a}$$

$$\frac{\partial \Theta_{-1}}{\partial t} = -\lambda Y_P \frac{V}{4}. \tag{3.15b}$$

The diffusion term is dropped since it is not essential for the destabilizing mechanism as seen in the preceding subsection. From (3.14) and (3.15), the equations for the time evolution of symmetric and antisymmetric modes can be easily derived:

$$\frac{\partial \overline{\Theta}}{\partial t} = 0, \tag{3.16}$$

$$\frac{\partial \hat{\Theta}}{\partial t} = \frac{\lambda}{4} Y_P^2 \hat{\Theta}, \tag{3.17}$$

where $\overline{\Theta} = \Theta_1 + \Theta_{-1}$ and $\hat{\Theta} = \Theta_1 - \Theta_{-1}$ represent the symmetric and antisymmetric modes, respectively. It follows that the symmetric mode is neutral, whereas the antisymmetric mode is unstable with a growth rate

$$\sigma = \frac{\lambda}{4} Y_P^2 = \frac{\lambda \beta}{4C} y_P^2. \tag{3.18}$$

The rotation of the earth is essential to the instability, both to its growth and antisymmetric structures. On a nonrotating sphere, the antisymmetric mode is neutral since $\sigma = 0$ for $\beta = 0$. In the above low-order model, the zonal wind induced by the same meridional flow (V) changes direction across the equator due to the change in sign of the Coriolis parameter, giving rise to the opposite signs on the right-hand sides of (3.15a) and (3.15b). This equatorially antisymmetric zonal wind field increases evaporation in one hemisphere but reduces it in the other under an easterly basic state, enhancing the existing antisymmetric SST distribution.

Low-order models have been shown to be a powerful tool for understanding the ENSO (Suarez and Schopf 1988; Battisti and Hirst 1989) and the zonal variations of the mean climate (Neelin and Dijkstra 1995). The present low-order model uses the minimum freedom—one SST grid point in each hemisphere—to represent the antisymmetric structure of the dominant WES instability mode. Despite the severe truncation, the low-order model captures the essence of the unstable growing mechanism seen in the numerical models and gives right functional dependence on external parameters. Here, we compare the low-order model with the linear numerical solution in terms of the dependence on the width of the coupling window. Figure 9 shows the growth rate of the WES mode obtained numerically with the full linear model as a function of Y_P. The growth rate increases with the expansion of the coupling window as predicted by the low-order model. The steeper than linear increase of the growth rate is also in a qualitative agreement with the quadratic function given in (3.18). Quantitatively, however, the growth rate based on the low-order model could vary depending on the discretizing scheme. We must be cautious about the quantitative features of the low-order model and use it for qualitative discussions only.

The WES instability occurs only with a basic state of prevalent easterly winds. In a zonally uniform setting,

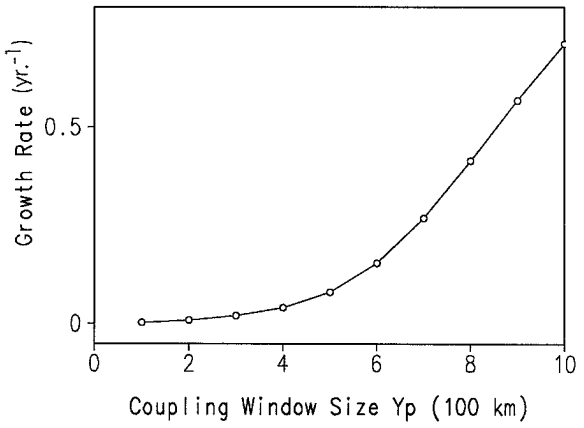

FIG. 9. Growth rate of the linear numerical solution as a function of the coupling window size.

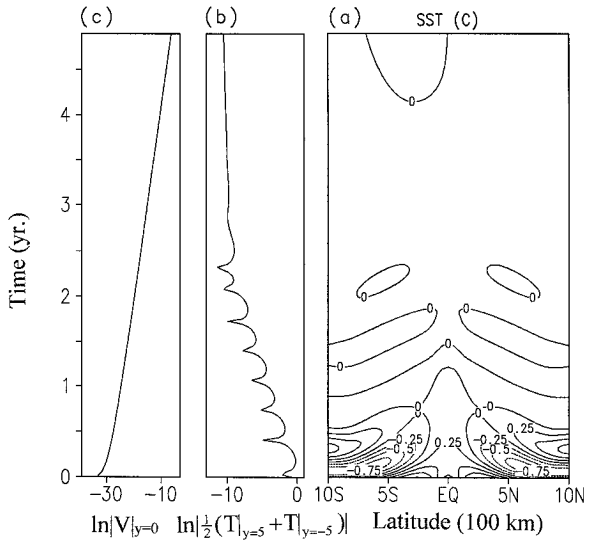

FIG. 10. (a) Time–latitude evolution of sea surface temperature of an initially symmetric disturbance (negative contours dashed), logarithms of (b) the average of SSTs at 5°S and 5°N, and (c) meridional wind speed at the equator as functions of time.

westerly winds in the Tropics are not possible due to the global angular momentum balance requirement. In a zonally asymmetric world, however, westerlies can dominate part of the equatorial belt as a result of the formation of the Walker circulation. The annual-mean westerlies in the Indian Ocean are such an example. With the mean winds being westerly, the effective coupling coefficient λ is negative in (3.10) and so is the growth rate of the WES mode according to (3.18). This prevents equatorial asymmetries from developing in the Indian Ocean, consistent with the more or less symmetric climate observed.

c. Evolution of a symmetric disturbance

The time evolution of symmetric disturbances is very different from that of the asymmetric ones. Figure 10 shows such an example. Everything but the initial conditions, including the model equations and parameters, is the same as the case shown in Fig. 4. The initial conditions are derived from the WES mode by filling the Northern Hemisphere with the mirror image of the modal structures in the Southern Hemisphere. This ensures that the initial disturbance is symmetric about the equator. This equatorially symmetric disturbance decays rapidly with time. The exponential decay can be seen clearly by tracing the time evolution of the average of SSTs at 5°N and 5°S (Fig. 10b), which serves as an index of the amplitude of the symmetric disturbances. Equatorward propagation can be seen in the time-latitude section (Fig. 10a), which causes the oscillations on the general trend of exponential decay in Fig. 10b. The diffusion in the numerical model is small and not enough to explain the rapid decay. The calculation of the destabilizing term $U'T'$ shows that it is negative in most parts of the domain and is responsible for the rapid decay of the symmetric disturbances. It is interesting to note that the oscillatory, fast decaying mode is replaced by a much more slowly decaying mode after three years in Fig. 10b, indicating the existence of two symmetric modes with different damping rates. The fast decaying mode initially has a larger amplitude but is overwhelmed by the slowly decaying one after a great loss of amplitude. While the equatorially symmetric disturbances decay rapidly with time, antisymmetric disturbances, arising from the round-off errors as discussed in section 2, grow exponentially. The growth of the antisymmetric mode is not visible for quite a long time from the time–latitude evolution of the total SST field (Fig. 10a), but is clear in the time evolution of the meridional wind speed at the equator (Fig. 10c). The exponential growth of the antisymmetric mode and the exponential decay of the symmetric disturbances ensure that the former will take over and dominate eventually. The equatorially asymmetric features become visible toward the end of the five-year calculation even in the SST field (Fig. 10a).

4. An alternative coupling approach

The latent heating associated with deep convection in the ITCZ is highly energetic and its effects dominate the whole Hadley circulation. It is certainly a major driving force to the surface winds throughout the Tropics. Since deep convection occurs only in a small area compared to vast downwelling regions and since it is strongly correlated with SST, the feedback from the SST to the atmosphere is confined to a small window where active deep convection occurs. Xie and Philander's (1994) model is constructed based upon this atmospheric forcing mechanism. This is not the whole story, however. In the regions of strong downdraft, temperature inversion occurs on the top of the planetary boundary layer, hampering its communications with the atmo-

sphere above. In such a situation, the SST may directly affect the temperature and thus winds within the boundary layer (Lindzen and Nigam 1987). Quantitative estimate of the contribution from this direct boundary layer forcing by SST in the real atmosphere, compared to the ITCZ forcing, is not well established from the observations. At this time, it seems instructive to explore the behavior of our linear model in the limit where the SST gradient acting on the planetary boundary layer is the only driving force. This limit allows the coupling between the ocean and atmosphere to occur everywhere, corresponding to an infinitely large coupling window, $Y_E = 0$ and $Y_p = \infty$, or $F(Y) = 1$. This section presents analytical and numerical solutions for $Y_p = \infty$ and a spatially constant λ.

Solutions to (3.7b) and (3.8) are sought of the form

$$\begin{Bmatrix} V \\ \Theta \end{Bmatrix} = \begin{Bmatrix} \tilde{V}(Y) \\ \tilde{\Theta}(Y) \end{Bmatrix} e^{\omega t}, \tag{4.1}$$

where ω is the growth rate and may take on complex values. Substitution of (3.8) into (3.7b) with the help of (4.1) leads to

$$\frac{d^2\tilde{V}}{dY^2} + 2\alpha Y\frac{d\tilde{V}}{dY} + (2\alpha - Y^2)\tilde{V} = 0, \tag{4.2}$$

where

$$\alpha = \frac{\lambda}{2\omega}. \tag{4.3}$$

A variable transformation,

$$\tilde{V} = e^{-\alpha Y^2/2}v, \tag{4.4}$$

transforms (4.2) into

$$\frac{d^2v}{dY^2} + [\alpha - (1 + \alpha^2)Y^2]v = 0, \tag{4.5}$$

which has the same form as the equation that leads to the dispersion relation of the equatorial waves (Matsuno 1966). The solutions to (4.5) are the parabolic cylinder functions. If $(1 + \alpha^2)$ has a real part, the solutions that vanish as $Y \to \infty$ are

$$v_n = 2^{-n/2}H_n[(1 + \alpha^2)^{1/4}Y] \exp\left[-\frac{1}{2}(1 + \alpha^2)^{1/2}Y^2\right], \tag{4.6}$$

or

$$\tilde{V}_n = 2^{-n/2}H_n[(1 + \alpha^2)^{1/4}Y] \exp\left\{-\frac{1}{2}[\alpha + (1 + \alpha^2)^{1/2}]Y^2\right\}, \tag{4.7}$$

where H_n is the Hermite polynomial of order n. The eigenvalues

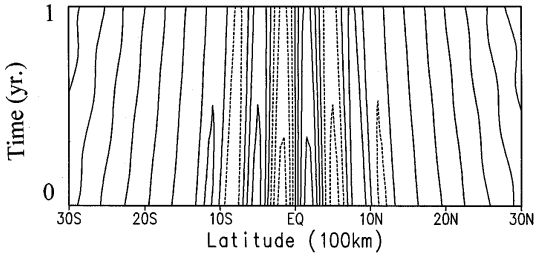

FIG. 11. Time–latitude section of sea surface temperature in a linear model with an infinite coupling window ($Y_p = \infty$, $\kappa = 2 \times 10^2$ m^2 s^{-1}, $K_Q = 2 \times 10^{-3}$ m^2 s^{-3} K^{-1}. Negative contours are dashed.

$$\alpha_n = \pm\frac{i}{2}\frac{2n + 1}{[n(n + 1)]^{1/2}}, \tag{4.8}$$

or

$$\omega_n = \mp i\frac{[n(n + 1)]^{1/2}}{2n + 1}\lambda, \qquad n = 1, 2, \ldots \tag{4.9}$$

are pure imaginary numbers. No instabilities exist and all solutions are neutral.

A problem with the eigenfunction (4.7) is that it does not approach zero as $Y \to \infty$. Since both α and $(1 + \alpha^2)^{1/2} = \pm i\{2[n(n+1)]^{1/2}\}^{-1}$ are pure imaginary numbers, the exponential function in (4.7) is not equatorially trapped, but is of wavy patterns of constant amplitude. This problem can be solved by removing the long-wave approximation in the atmospheric model. The counterpart of (3.7b) without imposing the long-wave approximation is (3.7a). The eigenvalue problem with (3.7b) replaced by (3.7a) can be solved in the same way. The eigenvalues are

$$\alpha_n = -\frac{\epsilon^2}{4n(n + 1)} \pm \frac{i}{2}\frac{2n + 1}{[n(n + 1)]^{1/2}}\left[1 - \frac{\epsilon^4}{4n(n + 1)}\right]^{1/2}, \tag{4.10}$$

which have a negative real part. As a result, the eigenmodes are weakly damped and trapped by the equator. In practice, however, the temperature diffusion is more effective in producing the equatorial trapping.

The local wavelength of the eigenmode (4.7) as measured by the distance of two neighboring zeroes decreases rapidly with latitude. A finite diffusivity can lead to an equatorially trapped structure by dampening the mode more at high latitudes than at low latitudes. Figure 11 shows the time–latitude section of a numerical solution with a finite diffusivity $\kappa = 2 \times 10^2$ m^2 s^{-1} in a larger oceanic domain, $|y| < 24\,000$ km. With an infinite coupling window ($Y_p = \infty$), a large domain is necessary. The numerical solution would be sensitive to the size of the domain if the domain is not large enough, in contrast to the finite coupling window case in section 3, where the numerical solution is neither sensitive to the size of the model domain nor to the space stepping.

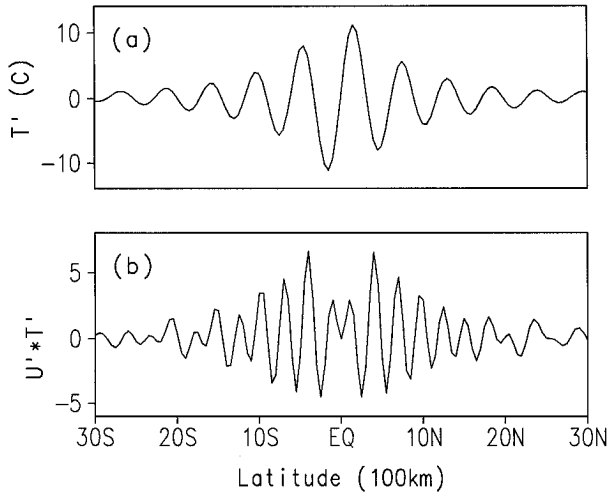

FIG. 12. (a) Sea surface temperature and (b) destabilizing term on day 360 of Fig. 11 as functions of time.

The model is initialized with a temperature field that is uniformly zero in the southern and 0.1°C in the Northern Hemisphere. The model is run for five years and the results in the last year are displayed. Weak decay of this disturbance is seen and its damping rate is 0.6 yr^{-1}. The spatial structures of the disturbance on the last day of Fig. 11 are depicted in Fig. 12, which are oscillatory in the meridional direction but trapped by the equator. These features are qualitatively in agreement with those of the analytical solutions, although a more detailed comparison requires an eigenvalue analysis in a system including the temperature diffusion term. The wavy patterns propagate toward the equator, a feature that is consistent with the analytical solution and has been extensively analyzed by Liu and Xie (1994). Away from the equator, the geostrophy prevails so that the zonal wind and SST disturbances maintain a phase difference of about 90°, with westerly equatorward and easterly winds poleward of a positive SST maximum. This 90° phase difference causes the whole structure to move equatorward. Liu and Xie propose that this equatorward propagating mode may carry equatorward the annual SST signals that are readily forced by the solar radiation in the off-equatorial region and may thus contribute to the genesis of the equatorial annual cycle.

The simple low-order model explains the WES instability under a finite coupling window, and successfully predicts the increase of the growth rate with the width of the coupling window in the parameter range shown in Fig. 9. The success of the simple low-order model cannot be extrapolated to the present case of infinite coupling window since the modal structures change into what a system of two temperature grid points cannot describe. It is these changes in the modal structure that transform the stationary WES instability into an oscillatory, damped mode as the coupling window expands. The meridional distribution of the destabilizing term $U'T'$ is displayed in Fig. 12b. Moving away from the equator, one first sees that $U'T'$ is positive by the mechanism described by the box model. Then comes negative $U'T'$ and the successive oscillatory patterns observed as one keeps moving poleward cancel each other. The integral of $U'T'$ over the latitudinal *e*-folding scale of the amplitude is negligible compared to the its local maxima, in contrast to the case with a finite equatorial coupling window in section 3a.

5. Discussion

A simple, one-dimensional ocean–atmosphere model is used to investigate the problem of latitudinal asymmetry of the ITCZ and the collocated SST maximum. Under conditions symmetric about the equator, a symmetric state with an SST minimum at the equator and double ITCZs—one in each hemisphere—is a solution to the coupled system. It is, however, unstable to infinitesimal disturbances and evolves into an equatorially asymmetric state described in Xie and Philander (1994). The unstable transition from the symmetric to the asymmetric state is due to the existence of an equatorially antisymmetric instability that is destabilized by a positive wind–evaporation–SST feedback. Similar unstable transition has been previously reported in a three-dimensional, hybrid coupled ocean GCM (Xie 1994b). In response to hemispherically symmetric solar radiation, atmospheric models with various complexities produce climates that may differ in various aspects but are symmetric about the equator (e.g., Numaguti and Hayashi 1991; Battisti and Ovens 1995). The existence of an antisymmetric coupled ocean–atmosphere instability indicates that upon being coupled with the ocean, these latitudinally symmetric model climates may be unstable and the ocean–atmosphere system could move toward a new steady state that is asymmetric about the equator. The latitudinal asymmetry of the ITCZ has an important consequence for the tropical seasonal cycle. The permanent stay of the ITCZ to one side of the equator has been shown to be a necessary condition for an annual cycle to appear on the equator where the annual component of the solar radiation vanishes (Xie 1994c).

The antisymmetric instability found in the nonlinear model is shown to be essentially linear and is reproduced in a model linearized around the symmetric steady-state solution. The destabilizing mechanism for this instability may be summarized in the schematic shown in Fig. 13a. In response to an SST disturbance that is negative to the north and positive to the south of the equator, northerly winds form. Because of the Coriolis force, these northerly winds induce easterly zonal winds to the north and westerlies to the south of the equator. Superimposed on prevalent easterly trade winds, this equatorially asymmetric zonal wind field amplifies the negative and positive SST anomalies in the Northern and Southern Hemispheres, respectively, through surface evaporation. Since it is the antisymmetric SST field that

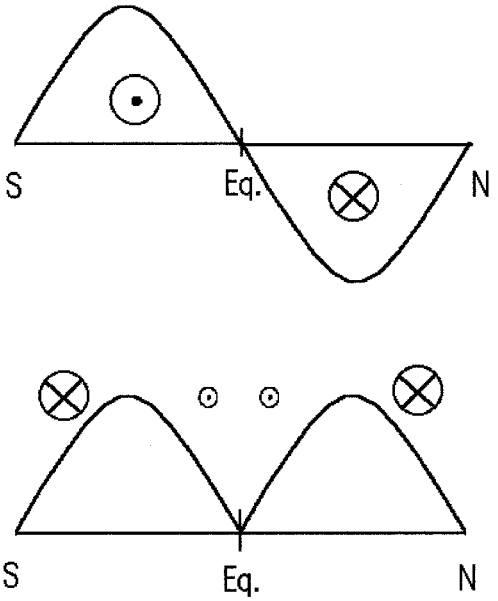

FIG. 13. Schematics of (a) antisymmetric and (b) symmetric coupled disturbances. The direction of the zonal wind is shown by the head or the tail of an arrow and its speed by the size of the circle.

produces the northerly winds in the first place, the above ocean–atmosphere interactions form a closed positive feedback that we call WES. The feedback acting upon an equatorially symmetric disturbance is completely different. The atmospheric response to a positive, symmetric SST disturbance shown in Fig. 13b is such that the westerly wind anomalies are weak and confined to a narrow equatorial region, whereas the easterlies are strong and occupy the rest of the Tropics. These strong easterlies increase the ocean heat loss by enhancing surface evaporation and thus act to dampen the initial SST disturbance. The asymmetry in the time-evolution characteristics between the equatorially symmetric and asymmetric disturbances is due to the rotation of the earth. The sign change of the Coriolis parameter across the equator is shown to be essential to the growth of the antisymmetric mode, as illustrated with a simple box model that consists of only two SST grid points, one in each hemisphere. The above destabilizing mechanism is valid only for a basic state of easterly winds. For westerly prevalent winds, the antisymmetric mode is damped, while the symmetric mode grows.

The persistent northerly ITCZ is not observed everywhere along the equator. In the Indian and western Pacific Oceans, SST and precipitation are to a large degree symmetrically distributed about the equator. The zonal distribution of the WES instability could be a possible reason for the observed geographic variation in the latitudinal asymmetry of the ITCZ. The negative growth rate in the Indian Ocean due to the prevalent westerlies prevents latitudinal asymmetry from developing. In the Pacific, the thermocline and mixed layer deepen in the west but shallow in the east in response to the mean easterly trade winds. The deep mixed layer and light annual-mean winds in the western Pacific weaken the ocean–atmosphere coupling and may not allow a WES mode to be unstable. On the other hand, in the eastern Pacific where the mixed layer depth is small, the WES mode gains a positive growth rate and sets the ITCZ in the Northern Hemisphere, presumably with the guide of such geographic asymmetries as those in the land mass distribution. To adequately address the problem of zonal variations, however, a model that includes the zonal dimension is necessary (Xie 1996).

Deep convection in the ITCZ, releasing enormous latent heating to the atmosphere, occurs only in regions with SSTs higher than a certain value. The area where the SST exceeds the threshold forms a window where the SST can affect the heating to the atmosphere. Outside the window, the ocean–atmosphere coupling is shut off. The spatially stationary antisymmetric instability occurs only when this coupling window is finite. The expansion of the coupling window leads to a weakly damped, equatorward propagating mode that is consistent with an eigenvalue analysis. The change in the time evolution characteristics arise from the changes in the modal structure. The phase relation between the zonal wind and SST changes from 0° near the equator to 90° in the off-equatorial regions where the geostrophy prevails. A perfect in-phase relation between the two fields causes a stationary instability, whereas a 90° phase difference leads to neutral propagating modes. Limiting the coupling to an equatorial window ensures an in-phase relation between the SST and the wind, leading to the destabilization of asymmetric disturbances. The size of the coupling window depends on the driving mechanism of the surface wind. In an atmosphere as described by Lindzen and Nigam's (1987) model, where the pressure gradient above the trade inversion vanishes and the SST-induced pressure gradient in the planetary boundary layer is the only driving force of the surface wind, the SST affects the surface wind everywhere, corresponding to an infinitely large coupling window. In an atmosphere where the ITCZ forcing is predominant, on the other hand, the coupling window is confined by the SST criterion. Certainly, both the ITCZ and boundary layer SST forcings are nonzero in the real atmosphere. Relative contribution from these two types of forcing to the surface winds is, however, difficult to determine since they produce very similar wind fields (Neelin 1989). Such a knowledge is necessary to determine the regime of the real atmosphere–ocean system in terms of its WES stability.

Surface evaporation occurs everywhere over the ocean, and its dependence on the wind speed is well established both in laboratory and field observations. Previous simple and intermediate coupled models, which have yielded great insights into the genesis of ENSO (see Philander 1990; McCreary and Anderson 1991; Neelin et al. 1994 for reviews), however, treat surface evaporation and the ocean heat flux simplisti-

cally as a Newtonian cooling with prescribed equilibrium temperature fields. Such a simplistic treatment eliminates the WES feedback. As evident from (3.2), the equilibrium temperature for the Newtonian cooling is a function of surface wind speed and is determined by ocean–atmosphere interaction. Xie (1994a) shows with an ocean GCM that among the various effects of wind forcing the latitudinal asymmetry in the scalar wind speed is the primary cause of the asymmetry in the SST field. In addition to the WES feedback described in this study, other feedback mechanisms can also possibly contribute to equatorial asymmetry. For example, SST and stratus clouds can form a local positive feedback over cold water; a negative SST anomaly causes an increase in the amount of stratus, which cools the ocean even more (Philander et al. 1996). A feedback mechanism described by Lau (1981) and Yamagata (1985), where the surface winds affect SST through upwelling and downwelling, can cause equatorially antisymmetric instabilities (Chang and Philander 1994). These two feedback mechanisms seem to be most effective near the east end of the Pacific where the low SST required to form stratus and shallow thermocline required for the upwelling to affect SST are observed. Despite these differences in conditions to operate, the WES and other mechanisms are complementary in producing and maintaining the latitudinal asymmetry of the coupled ocean–atmosphere system.

Acknowledgments. I would like to thank Kirk Bryan at Princeton University for discussions that have led to the idea of developing a low-order model, Atsushi Kubokawa at Hokkaido University for valuable discussions and comments, and the anonymous referees for comments that helped improve the manuscript. Several figures are produced using the GrADS developed by Brian Doty at University of Maryland. This work was supported by grants from the Japanese Ministry of Education, Culture and Science, and from the Center for the Climate System Research of the University of Tokyo.

REFERENCES

Battisti, D. S., and A. C. Hirst, 1989: Interannual variability in a tropical atmosphere–ocean model: Influence of the basic state, ocean geometry, and nonlinearity. *J. Atmos. Sci.,* **46,** 1687–1712.

——, and D. W. Ovens, 1995: The dependence of the low-level equatorial easterly jet on the Hadley and Walker circulations. *J. Atmos. Sci.,* **52,** 3911–3931.

Chang, P., and S. G. H. Philander, 1994: A coupled ocean–atmosphere instability of relevance to the seasonal cycle. *J. Atmos. Sci.,* **51,** 3627–3648.

Lau, K. M., 1981: Oscillations in a simple equatorial climate system. *J. Atmos. Sci.,* **38,** 248–261.

Lindzen, R. S., and S. Nigam, 1987: On the role of sea surface temperature gradients in forcing low-level winds and convergence in the tropics. *J. Atmos. Sci.,* **44,** 2418–2436.

Liu, Z., and S.-P. Xie, 1994: Equatorward propagation of coupled air–sea disturbances with application to the annual cycle of the eastern tropical Pacific. *J. Atmos. Sci.,* **51,** 3807–3822.

Manabe, S., D. G. Hahn, and J. L. Holloway, 1974: The seasonal variation of the tropical circulation as simulated by a global model of the atmosphere. *J. Atmos. Sci.,* **31,** 43–83.

Matsuno, T., 1966: Quasi-geostrophic motions in the equatorial area. *J. Meteor. Soc. Japan,* **44,** 25–43.

McCreary, J. P., and D. L. T. Anderson, 1991: An overview of coupled ocean–atmosphere models of El Niño and the Southern Oscillation. *J. Geophys. Res.,* **96,** 2125–3150.

Neelin, J. D., 1989: On the interpretation of the Gill model. *J. Atmos. Sci.,* **46,** 2466–2468.

——, and H. A. Dijkstra, 1995: Ocean–atmosphere interaction and the tropical climatology. Part I: The dangers of flux correction. *J. Climate,* **8,** 1325–1342.

——, M. Latif, and F.-F. Jin, 1994: Dynamics of coupled ocean–atmosphere models: The tropical problem. *Annu. Rev. Fluid Mech.,* **26,** 617–659.

Numaguti, A., and Y.-Y. Hayashi, 1991: Behavior of cumulus activity and the structures of circulations in an ''aqua-planet'' model. Part II: Eastward-moving planetary scale structure and the Intertropical Convergence Zone. *J. Meteor. Soc. Japan,* **69,** 563–579.

Philander, S. G. H., 1990: *El Niño, La Niña, and the Southern Oscillation.* Academic Press, 293 pp.

——, G. Lambert, T. Li, N.-C. Lau, and D. Halpern, 1996: Why the ITCZ is mostly north of the equator. *J. Climate,* **9,** 2958–2972.

Suarez, M. J., and P. Schopf, 1988: A delayed action oscillator for ENSO. *J. Atmos. Sci.,* **45,** 3283–3287.

Xie, S.-P., 1994a: Oceanic response to the wind forcing associated with the Intertropical Convergence Zone in the Northern Hemisphere. *J. Geophys. Res.,* **99,** 20 393–20 402.

——, 1994b: The maintenance of an equatorially asymmetric state in a hybrid coupled GCM. *J. Atmos. Sci.,* **51,** 2602–2612.

——, 1994c: On the genesis of the equatorial annual cycle. *J. Climate,* **7,** 2008–2013.

——, 1996: Westward propagation of latitudinal asymmetry in a coupled ocean–atmosphere model. *J. Atmos. Sci.,* **53,** 3236–3250.

——, and S. G. H. Philander, 1994: A coupled ocean–atmosphere model of relevance to the ITCZ in the eastern Pacific. *Tellus,* **46A,** 340–350.

Yamagata, T., 1985: Stability of a simple air–sea coupled model in the tropics. *Coupled Ocean–Atmosphere Models,* J. C. J. Nihoul, Ed., Elsevier Oceanography Series, Vol. 40, Elsevier, 637–657.